Ion distributions, exclusion coefficients, and separation factors of electrolytes in a charged cylindrical nanopore: A partially perturbative density functional theory study

Bo Peng and Yang-Xin Yu[a)]
Department of Chemical Engineering, Tsinghua University, Beijing 100084, People's Republic of China and State Key Laboratory of Chemical Engineering, Tsinghua University, Beijing 100084, People's Republic of China

(Received 17 February 2009; accepted 15 September 2009; published online 6 October 2009)

The structural and thermodynamic properties for charge symmetric and asymmetric electrolytes as well as mixed electrolyte system inside a charged cylindrical nanopore are investigated using a partially perturbative density functional theory. The electrolytes are treated in the restricted primitive model and the internal surface of the cylindrical nanopore is considered to have a uniform charge density. The proposed theory is directly applicable to the arbitrary mixed electrolyte solution containing ions with the equal diameter and different valences. Large amount of simulation data for ion density distributions, separation factors, and exclusion coefficients are used to determine the range of validity of the partially perturbative density functional theory for monovalent and multivalent counterion systems. The proposed theory is found to be in good agreement with the simulations for both mono- and multivalent counterion systems. In contrast, the classical Poisson–Boltzmann equation only provides reasonable descriptions of monovalent counterion system at low bulk density, and is qualitatively and quantitatively wrong in the prediction for the multivalent counterion systems due to its neglect of the strong interionic correlations in these systems. The proposed density functional theory has also been applied to an electrolyte absorbed into a pore that is a model of the filter of a physiological calcium channel. © *2009 American Institute of Physics*. [doi:10.1063/1.3243873]

I. INTRODUCTION

The structural and transport properties of electrolytes confined in charged nanopores differ greatly from their bulk behavior due to the interplay between charged wall-ion and ion-ion interactions.[1] Generally, there is an excess of counterions inside the charged nanopore while co-ions are partly excluded from the region because of the charged groups on the internal wall. This is of great interest in chemical science and plays an important role in several separation processes such as desalination of water[2] and convective electrophoresis in porous membranes.[3] Further examples include zeolites[4] and ion channels through membranes.[5] In the latter case, ion partitioning provides considerable physiological implications. So far both the Monte Carlo (MC)[6–11] and molecular dynamics[12] simulations have been used to investigate the ion density distributions, ion partitioning, and transport of various model electrolytes in charged cylindrical nanopores. Nevertheless, the molecular simulations are usually time consuming and numerically involved. In order to understand the processes in the charged nanopore and quantitatively analyze experimental data, it is necessary to construct a statistical mechanical theory to relate the measurable quantities to the molecular properties of electrolyte solution (i.e., ion size and valence) and pore parameters (i.e., pore diameter and surface charge density).

The simplest description of ion partitioning between charged nanopore and bulk electrolyte solution is on the basis of the classical Donnan equilibrium.[13] The Donnan theory[13] greatly overestimates the rejection of electrolyte solutions and cannot explain the enrichment of electrolyte in systems with multivalent counterions.[14] A more detailed theory for the electrolyte exclusion is the so-called Poisson–Boltzmann (PB) equation.[15] Although the PB equation has been successful in describing experimental results for monovalent counterion systems in the cylindrical nanopores with moderate surface charge densities, it breaks down when divalent counterions are present in the nanopore[6,7,9] due to its neglect of ion size and the correlations between ions. A more accurate theory is still in demand for the analysis of the membrane experimental data.

Some efforts have been made to improve the description of electrolyte exclusion in the charged cylindrical nanopores. These include the modified PB (MPB) theory,[16] the hypernetted-chain/mean spherical approximation (HNC/MSA) theory,[17] and density functional theory (DFT).[18] Beyond the PB equation, the MPB theory takes the ion size and interionic correlations into account in a potential formulation.[19] In both HNC/MSA theory and DFT, the interionic correlations are considered by the Ornstein–Zernike integral equation with the MSA.[20] Although both the MPB and HNC/MSA theories are comparable to the partially perturbative DFT in describing the structure of electric double layer, the DFT possesses several advantages. For example,

[a)]Author to whom correspondence should be addressed. Electronic mail: yangxyu@mail.tsinghua.edu.cn.

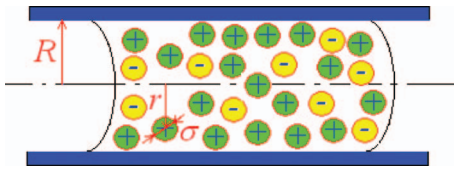

FIG. 1. Cross section through the charged cylindrical nanopore.

the DFT can be easily implemented for other interactions between ions and directly extended to multicomponent systems. When compared with the molecular simulation data, several versions of DFT were found to be accurate for the structural and thermodynamic properties of the planar,[21] spherical,[22] and cylindrical[23,24] double layers. However, few DFTs are applied to the cylindrical nanopores with surface charge in the internal wall. Only Busath *et al.*[18] used DFT to investigate the ions confined in a charged cylindrical nanopore. In their study, the cylindrical nanopore was selected as a model of the calcium channel. They found that the nanopore behaves as a calcium channel filter and selectively adsorbs calcium ions in preference to sodium ions when the charged density on the pore wall corresponds to six half-charged oxygen "ions" smeared over the surface of a cylindrical pore length of 0.75 nm. The ion density profiles of Na^+, Ca^{2+}, and Cl^- as well as electrostatic potentials inside the cylindrical nanopore were also obtained. It is of interest to apply the partially perturbative DFT we developed previously for inhomogeneous electrolyte solutions to the cylindrical confinement.

In this paper, the partially perturbative DFT, which is based on the modified fundamental measure theory[25] for hard-core repulsion contribution and a functional Taylor expansion of the charge contribution around the uniform reference fluid,[26] is applied to investigating the ion density profiles, exclusion coefficients, and separation factors of various electrolytes inside charged cylindrical nanopores. The structure and thermodynamics are examined as a function of the surface charge density and composition for charge symmetric and asymmetric model electrolytes as well as for charge asymmetric mixture with a common ion (i.e., MX_2-NX-H_2O system). Although this work only concerns the electrolytes with an equal ion diameter (i.e., restricted primitive model), the approach should be applicable to the electrolytes with different ion diameters.[27]

II. MODEL AND THEORY

A. Model

The model used in this work is the same as in several previous studies.[6,7,9] The porous material is pictured as a collection of equal cylindrical nanopores with radius R, which do not interact with each other. The cylindrical nanopore shown in Fig. 1 is assumed to be very long and has a uniform charge density on its internal surface. The electrolyte in the nanopore is assumed to be in equilibrium with a bulk electrolyte of the same chemical composition. The interaction between two ions of species i and j is given by

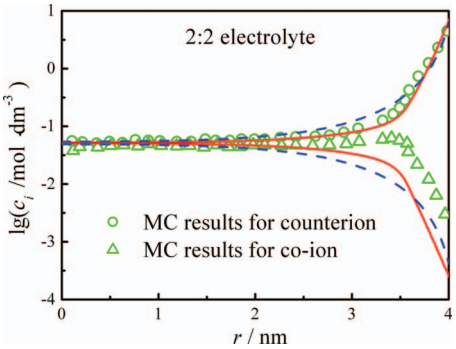

FIG. 2. Local concentrations of co-ion and counterion for 2:2 electrolyte inside a charged cylindrical pore with radius $R=4.2125$ nm at temperature $T=298$ K. Here the bulk electrolyte concentration is $c_b=0.0515$ mol dm^{-3}, the ion diameter is $\sigma=0.425$ nm, and the capillary surface charge density is $Q=-0.1422$ C/m^2. The symbols (circles for counterion and triangles for co-ion) and dashed and solid lines represent the results from the MC simulations (Ref. 9), PB equation, and present DFT, respectively.

$$u_{ij}(r)=\begin{cases}\infty & r<\sigma_{ij}\\ \dfrac{z_i z_j e^2}{4\pi\varepsilon_0\varepsilon r} & r>\sigma_{ij}\end{cases}, \tag{1}$$

where $\sigma_{ij}=(\sigma_i+\sigma_j)/2$, σ_i is the ion diameter, r is the distance between two ions, z_i is the valence of an ion of type i, e is the electron charge, ε_0 is the vacuum permittivity, and ε is the dielectric constant of solvent water. In this work, the restrict primitive model of electrolyte is used, i.e., $\sigma_i=\sigma_j=\sigma$. All the calculations in Figs. 1–7 were carried out at temperature $T=298$ K and $\varepsilon=78.54$.

B. Density functional theory

In a DFT, the ion density profiles $\rho_i(\mathbf{r})$ inside the cylindrical nanopore are obtained by solving the Euler–Lagrange equations

$$\delta\Omega[\{\rho_i(\mathbf{r})\}]/\delta\rho_i(\mathbf{r})=0, \quad (i=1,2,\cdots), \tag{2}$$

which correspond to the minimization of the grand potential $\Omega[\{\rho_i(\mathbf{r})\}]$,

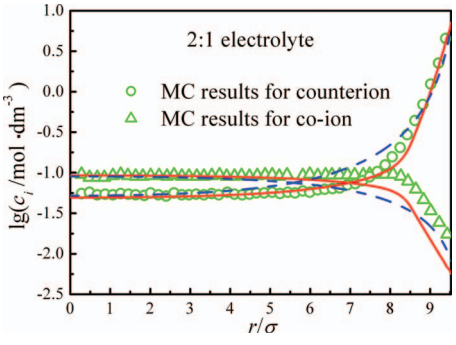

FIG. 3. Local concentrations of co-ion and counterion for 2:1 electrolyte (divalent counterion) inside a charged cylindrical pore with radius $R=4.21$ nm at temperature $T=298$ K. Here the bulk electrolyte concentration is $c_b=0.0475$ mol dm^{-3}, the ion diameter is $\sigma=0.42$ nm, and the nanopore surface charge density is $Q=-0.1425$ C/m^2. The symbols (circles for counterion and triangles for co-ion) and dashed and solid lines represent the results from the MC simulations (Ref. 6), PB equation, and present DFT, respectively.

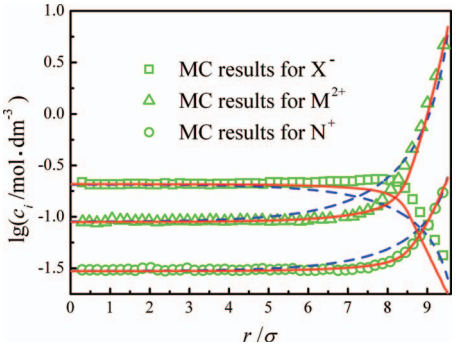

FIG. 4. Local concentrations of co-ion and counterions inside a charged cylindrical pore with radius $R=4.21$ nm for MX_2-NX-H_2O system at temperature $T=298$ K. Here the ionic strength of the bulk solution is $I=0.2965$ mol dm^{-3}, the ion diameter is $\sigma=0.42$ nm, the ionic strength fraction of MX_2 is $x_{MX}=0.9$, and the surface charge density $Q=-0.1425$ C/m^2. The symbols and dashed and solid lines represent the results from the MC simulations (Ref. 7), PB equation, and present DFT, respectively.

$$\Omega[\{\rho_i(\mathbf{r})\}] = F^{\mathrm{id}} + F^{\mathrm{ex}} + \sum_i \int d\mathbf{r}\rho_i(\mathbf{r})[V_i^{\mathrm{ext}}(\mathbf{r}) - \mu_i], \quad (3)$$

where μ_i is the chemical potential of component i, $V_i^{\mathrm{ext}}(\mathbf{r})$ is the external potential arising from the pore wall, F^{id} and F^{ex} represent, respectively, the ideal and excess parts of the Helmholtz energy functional. F^{id} is given by the exact relation

$$F^{\mathrm{id}}[\rho(\mathbf{r})] = k_B T \sum_i \int d\mathbf{r}\rho_i(\mathbf{r})[\ln\{\rho_i(\mathbf{r})\lambda_i^3\} - 1], \quad (4)$$

where λ_i is the de Broglie thermal wavelength, and k_B is the Boltzmann constant. Without loss of generality, F^{ex} can be decomposed as

$$F^{\mathrm{ex}} = F^{\mathrm{hs}} + F^{\mathrm{cor}} + F^{\mathrm{C}}, \quad (5)$$

where F^{hs}, F^{cor}, and F^{C} are the excess Helmholtz energy functional contributed by hard-core repulsive, interionic correlations, and Coulombic interactions, respectively. Among the free energy functional model for the hard-sphere fluid,

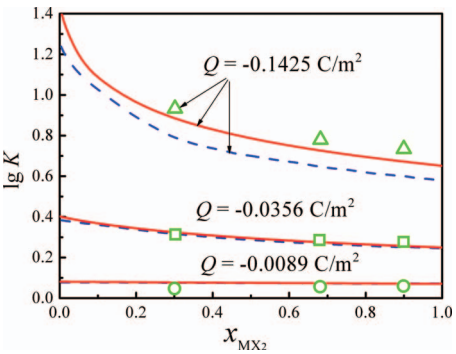

FIG. 5. The separation factors K as a function of the ionic strength fraction of MX_2 for MX_2-NX-H_2O system inside a charged cylindrical pore with radius $R=4.21$ nm at temperature $T=298$ K. Here the ionic strength of the bulk solution is $I=0.1496$ mol dm^{-3}, the ion diameter is $\sigma=0.42$ nm, and the surface charge density is $Q=-0.0089$, -0.0356, and -0.1425 C/m^2. The symbols and dashed and solid lines represent the results from the MC simulations (Ref. 7), PB equation, and present DFT, respectively.

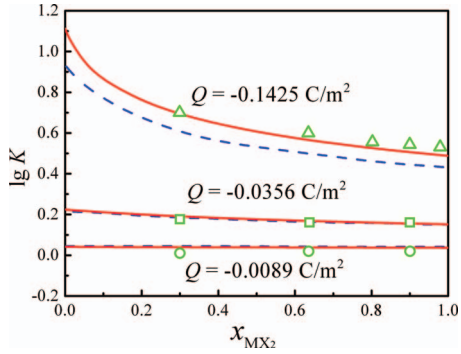

FIG. 6. The same as in Fig. 6 except for the ionic strength of the bulk solution $I=0.2965$ mol dm^{-3}.

the modified fundamental measure theory[25] is the most accurate one and thus it is adopted in this paper.

$$F^{\mathrm{hs}} = k_B T \int \Phi^{\mathrm{hs}}[\{n_\alpha(\mathbf{r})\}]d\mathbf{r}, \quad (6)$$

where $\Phi^{\mathrm{hs}}[\{n_\alpha(\mathbf{r})\}]$ is the excess Helmholtz free-energy density due to hard-core repulsion. It consists of scalar (S) and vector (V) parts,

$$\Phi^{\mathrm{hs}}[\{n_\alpha(\mathbf{r})\}] = \Phi^{\mathrm{hs(S)}} + \Phi^{\mathrm{hs(V)}}. \quad (7)$$

According to the modified fundamental measure theory of Yu and Wu,[25] the scalar part is given by the Boublik–Mansoori–Carnahan–Starling–Leland equation of state[28]

$$\Phi^{\mathrm{hs(S)}} = -n_0 \ln(1-n_3) + \frac{n_1 n_2}{1-n_3} + \frac{n_2^3 \ln(1-n_3)}{36\pi n_3^2} + \frac{n_2^3}{36\pi n_3(1-n_3)^2}, \quad (8)$$

and the vector part is expressed as[25]

$$\Phi^{\mathrm{hs(V)}} = -\frac{\mathbf{n}_{V1}\cdot\mathbf{n}_{V2}}{1-n_3} - \frac{n_2\mathbf{n}_{V2}\cdot\mathbf{n}_{V2}\ln(1-n_3)}{12\pi n_3^2} - \frac{n_2\mathbf{n}_{V2}\cdot\mathbf{n}_{V2}}{12\pi n_3(1-n_3)^2}. \quad (9)$$

The weighted densities in Eqs. (8) and (9) are defined as

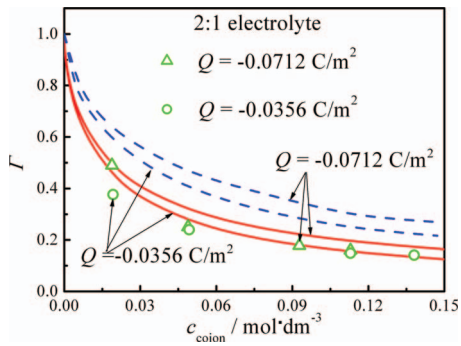

FIG. 7. Exclusion coefficients Γ for 2:1 electrolyte in inside a charged cylindrical nanopore ($R=4.21$ nm) as a function of concentration of co-ions in the external bulk electrolyte solution at temperature $T=298$ K. The symbols and dashed and solid lines represent the results from the GCMC simulations (Ref. 6), PB approximation, and present DFT, respectively.

$$n_\alpha(\mathbf{r}) = \sum_i \int d\mathbf{r}' \rho_i(\mathbf{r}') w_i^{(\alpha)}(\mathbf{r}-\mathbf{r}'), \tag{10}$$

where $\alpha=0,1,2,3$, V1, and V2. The weight functions, $w_i^{(\alpha)}(r)$, are defined by[25,29]

$$w_i^{(2)}(r) = \pi\sigma_i^2 w_i^{(0)}(r) = 2\pi\sigma_i w_i^{(1)}(r) = \delta(\sigma_i/2 - r), \tag{11}$$

$$w_i^{(3)}(r) = \Theta(\sigma_i/2 - r), \tag{12}$$

$$\mathbf{w}_i^{(V2)}(\mathbf{r}) = 2\pi\sigma_i \mathbf{w}_i^{(V1)}(\mathbf{r}) = (\mathbf{r}/r)\delta(\sigma_i/2 - r). \tag{13}$$

In Eqs. (11)–(13), $\Theta(r)$ is the Heaviside step function, and $\delta(r)$ denotes the Dirac delta function.

The Coulombic contribution to the excess Helmholtz energy functional is obtain via a mean-field approach,

$$F^C = \sum_i \int z_i e \psi(\mathbf{r}) \rho_i(\mathbf{r}) d\mathbf{r}, \tag{14}$$

where $\psi(\mathbf{r})$ is the electrostatic potential. It can be derived from Poisson equation. For ions confined in a charged cylindrical nanopore, it is given by

$$\psi(r) = \psi(R) + \sum_i \frac{z_i e}{\varepsilon_0 \varepsilon} \int_0^R \ln\left(\frac{R}{t}\right) \rho_i(t) t dt - \sum_i \frac{z_i e}{\varepsilon_0 \varepsilon} \int_0^r \ln\left(\frac{r}{t}\right) \rho_i(t) t dt. \tag{15}$$

The interionic correlation contribution to the excess Helmholtz energy functional is derived from a truncated second-order functional Taylor expansion around the corresponding bulk fluid.

$$F^{\text{cor}} = F^{\text{cor}}(\{\rho_i^b\}) + \sum_i \int \frac{\delta F^{\text{cor}}}{\delta \rho_i(\mathbf{r})} \Delta\rho_i(\mathbf{r}) d\mathbf{r} + \frac{1}{2}\sum_i \sum_j \int\int d\mathbf{r}' d\mathbf{r} \frac{\delta^2 F^{\text{cor}}}{\delta\rho_i(\mathbf{r})\delta\rho_j(\mathbf{r}')} \Delta\rho_i(\mathbf{r})\Delta\rho_j(\mathbf{r}') + \cdots, \tag{16}$$

where $\Delta\rho_i(\mathbf{r}) = \rho_i(\mathbf{r}) - \rho_i^b$, and ρ_i^b is the bulk density of ion species i. The direct correlation functions due to the interionic correlations are defined as

$$\Delta C_i^{(1)}(\mathbf{r}) = -\beta \delta F^{\text{cor}} / \delta \rho_i(\mathbf{r}), \tag{17}$$

$$\Delta C_{ij}^{(2)}(|\mathbf{r}' - \mathbf{r}|) = -\beta \delta^2 F^{\text{cor}} / \delta\rho_i(\mathbf{r}) \delta\rho_j(\mathbf{r}'), \tag{18}$$

where $\beta = 1/k_B T$. If we neglect all higher-order terms $\Delta C^{(n)}$ $(n>2)$ in Eq. (16), F^{cor} becomes

$$\beta F^{\text{cor}} = \beta F^{\text{cor}}(\{\rho_i^b\}) - \sum_i \int \Delta C_i^{(1)}(\mathbf{r}) \Delta\rho_i(\mathbf{r}) d\mathbf{r} - \frac{1}{2}\sum_i \sum_j \int\int d\mathbf{r}' d\mathbf{r} \Delta C_{ij}^{(2)}(|\mathbf{r}' - \mathbf{r}|) \Delta\rho_i(\mathbf{r}) \Delta\rho_j(\mathbf{r}'). \tag{19}$$

Once the expressions for each part of Helmholtz energy functional are known, the following Euler–Lagrange equations for the ion density profiles can be achieved from Eq. (1).

$$\ln\left[\frac{\rho_i(r)}{\rho_i^b}\right] = \beta\left[\mu_i^{\text{hs}} - \frac{\delta F^{\text{hs}}}{\delta\rho_i(\mathbf{r})}\right] - \beta V_i^{\text{hw}}(r) - z_i e \beta\psi(r) + \sum_j \int \Delta C_{ij}^{(2)}(|\mathbf{r}' - \mathbf{r}|) \Delta\rho_j(\mathbf{r}') d\mathbf{r}', \tag{20}$$

where

$$V_i^{\text{hw}}(r) = \begin{cases} \infty & r > R - \sigma_i/2 \\ 0 & r < R - \sigma_i/2 \end{cases} \tag{21}$$

is the hard-cylindrical wall external potential, and μ_i^{hs} is the hard-sphere part of chemical potential of ion of species i. In this work, the second-order direct correlation functions are obtained from the Ornstein–Zernike integral equation with the MSA,[30]

$$\Delta C_{ij}^{(2)}(r) = \begin{cases} -\dfrac{\beta z_i z_j e^2}{4\pi\varepsilon_0\varepsilon}\left[\dfrac{2B}{\sigma} - \left(\dfrac{B}{\sigma}\right)^2 r - \dfrac{1}{r}\right] & r < \sigma \\ 0 & r > \sigma \end{cases}, \tag{22}$$

where $B = [y^2 + y - y(1+2y)^{1/2}]/y^2$ with $y^2 = (\beta\sigma^2/\varepsilon_0\varepsilon)\Sigma_i \rho_i^b z_i^2 e^2$.

The numerical technique used to solve Eq. (20) is quite similar to our previous work.[22,23] In order to use the theory conveniently, the explicit expression of the numerical integral of the term containing the second-order direct correlation function in Eq. (20) is given in the Appendix. A standard Picard iteration procedure is adopted and we adjust $\psi(R)$ by trial and error until the charge of the ions in the cylindrical nanopore is equal in magnitude by opposite in the sign to that on the internal surface of the nanopore, i.e., the electroneutrality holds inside the nanopore. The surface charge density on the internal surface of the cylindrical nanopore is obtained by

$$Q = -\sum_i \frac{z_i e}{R} \int_0^R \rho_i(r) r dr \tag{23}$$

III. RESULTS AND DISCUSSION

In this section we compare the predicted results from the present DFT with those from the MC simulations[6–9] and PB equation for various electrolyte solutions confined in the charged cylindrical nanopores. We considered three different ionic solutions in the nanopore, i.e., (i) 2:2 electrolyte, (ii) 2:1 electrolyte (divalent counterion), and (iii) MX_2-NX-H_2O system in the nanopore with negative surface charge density. For 2:2 electrolyte, the common ion diameter is $\sigma = 0.425$ nm. For 2:1 and mixed MX_2-NX electrolytes, the ion diameter is $\sigma = 0.42$ nm. In order to test the accuracy of the present DFT predictions against the computer simulation data, all the calculations were carried out under the same conditions as in the molecular simulations.[6–9]

A. Ion concentration profiles and electrostatic potentials

We consider the structural properties of electrolyte inside the charged cylindrical nanopores. The predicted ion concentration profiles from the present DFT along with those from the MC simulations and PB equation are presented in Figs. 2 and 3 for 2:2 and 2:1 electrolytes, respectively. In the divalent counterion systems, the distributions of both co-ion and counterion predicted from the present DFT are considerably more uniform in the major part of a nanopore than those from the PB equation. As a consequence, the present DFT predicts a thinner double layer and a lower electrostatic potential than the PB equation does. As can be seen from Figs. 2 and 3, strong correlations between divalent counterions and co-ions cause the local concentration of co-ion to be higher than that from the PB equation, which results in a lower electrostatic potential. Since the present DFT includes the effect of interionic correlations, its predictions are much closer to the MC simulation values. The underestimation of the local concentration of co-ion near the wall in Figs. 2 and 3 is possibly due to the approximation of analytical direct correlation functions from the MSA. A more accurate expression of direct correlation functions, e.g., from the generalized MSA (GMSA),[31] may improve the DFT predictions.

In Fig. 4, the local concentration profiles of co-ion and counterion predicted from the present DFT are compared with those from the GCMC simulations and PB equation for MX_2-NX-H_2O solution confined in the charged cylindrical nanopore at the ionic strength fraction $x_{MX}=0.9$. In these cases the performance of the present DFT and PB equation is similar to that for single 2:1 or 2:2 electrolyte system with a divalent counterion. Figure 4 shows that the DFT results are much closer to the GCMC simulation data than those predicted from the PB equation, but they still need to be improved. It is obviously seen in Fig. 4 that the PB equation has limited validity for the confined mixed electrolyte solution under these conditions.

B. Separation factor

The separation factor is an important quantity to represent the equilibrium between bulk mixed electrolyte solution and the ion-exchange resin.[32] A high value of separation factor indicates that the mixed electrolytes are easily separated by an ion-exchange membrane.[33] In general, the separation factor K for the mixed system MX_2-NX-H_2O is defined as

$$K=[\langle c_2\rangle_p/\langle c_1\rangle_p]/(c_2^b/c_1^b), \tag{24}$$

where $\langle c_2\rangle_p$ and $\langle c_1\rangle_p$ are the average concentrations of divalent counterion M^{2+} and monovalent counterion N^+ in a charged nanopore, respectively. Further, c_2^b and c_1^b are the concentrations of M^{2+} and N^+ in the corresponding bulk solution, respectively.

The separation factors predicted from the present DFT are compared with those from the GCMC simulations and PB equation in Figs. 5 and 6 for MX_2-NX-H_2O solution in a charged cylindrical nanopore at ionic strength $I=0.1496$ and 0.2965 mol dm^{-3}, respectively. The separation factor increases as the absolute value of the surface charge density is increased and decreases as the ionic strength fraction of the divalent counterion M^{2+} is increased. Both theories correctly predict the varying trends of the separation factor with the surface charge density and ionic strength fraction of divalent counterion in the bulk solution. At low absolute value of surface charge density, the two theories predict almost the same separation factor but the separation factors from the present DFT are much closer to the GCMC simulation data than those from the PB equation at high absolute value of surface charge density ($Q=-0.1425$ C/m^2). A comparison between Figs. 5 and 6 suggests that at same surface charge density, the charged cylindrical nanopore is more selective for divalent counterion M^{2+} when the total ionic strength of the bulk solution is lower. This is because, at the high ionic strength of the bulk solution, the electric double layer near the surface is thin and this makes the capillary loss the selective capacity to some extent. The separation factors predicted from the present DFT are in fair agreement with those from the GCMC simulations. This indicates that the interionic correlations are also important for the separation factor of mixed electrolyte solution inside the charged cylindrical nanopore, especially for high absolute values of surface charge density.

C. Exclusion coefficient

Due to the charge on the internal surface and the hard-wall depletion effect, the co-ions are partly excluded from the charged nanopore. As a result, a rejection of electrolyte is observed. Jamnik and Vlachy[6] suggested that the exclusion coefficient should be a convenient measure of this effect for the charged nanopores. In their study, the exclusion coefficient is defined by

$$\Gamma=[c_{\text{co-ion}}^b-\langle c_{\text{co-ion}}\rangle_p]/c_{\text{co-ion}}^b, \tag{25}$$

where $c_{\text{co-ion}}^b$ is the concentration of co-ion in the bulk electrolyte solution, and $\langle c_{\text{co-ion}}\rangle_p$ is the average concentration of co-ion in the charged cylindrical nanopore.

In Fig. 7, we compare the theoretical exclusion coefficients with those from the GCMC simulations for aqueous solution of 2:1 electrolyte in the nanopores. As can be seen in Fig. 7, both theories predict a decrease in exclusion coefficient with the increase in the concentration of co-ion in the bulk solution for 2:1 electrolyte, while the results from the present DFT are much closer to the GCMC simulation data than those from the PB equation. It is of interest to point out that the present DFT can be extended to arbitrary mixed electrolyte systems[27] where the cations and anions have different diameters using the direct correlation functions of the MSA derived by Hiroike.[34]

D. Selectivity of a calcium channel

In this section, we apply the present DFT to a model calcium channel described by Boda *et al.*[11,35] The electrolyte in the channel consists of Na^+, Ca^{2+}, Cl^-, and $O^{-1/2}$ ions. All the ions in the channel have a same diameter $\sigma=0.25$ nm. The solvent is represented by a dielectric continuum with a dielectric constant of water (78.5) at 300 K. The calculation was started with a 0.1M NaCl solution in the bulk and then

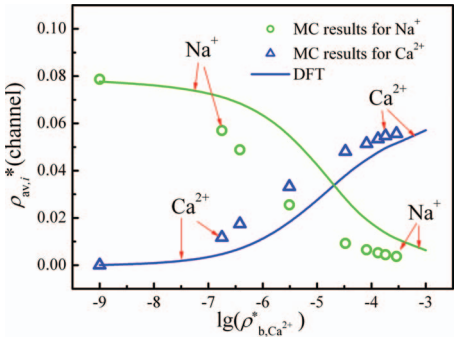

FIG. 8. Average ion densities in a model calcium channel as a function of the bulk density of Ca^{2+} ion for the two $O^{-1/2}$ ions ($\rho^*_{av,O^{-1/2}}=0.28$) in the channel at 300 K. The ions has a same diameter of 0.25 nm and the radius of the pore is $R=0.50$ nm. The symbols and curves represent the results from the MC simulations and present DFT, respectively.

incremental amounts of $CaCl_2$ were added to the bulk solution. Figure 8 depicts the average densities of Ca^{2+} and Na^+ ions in the channel as a function of the bulk Ca^{2+} ion density for two $O^{-1/2}$ ions ($\rho^*_{av,O^{-1/2}}=0.28$) in the channel. The results are compared with those from the MC simulations.

From Fig. 8 one can see that the average density of Ca^{2+} ion increases while the average density of Na^+ ion decreases rapidly as the concentration of $CaCl_2$ in the bulk is increased. The average density of Ca^{2+} ions in the channel exceeds that of Na^+ ions when the reduced bulk density of Ca^{2+} ions is about 2×10^{-5}. This value is somewhat greater than the corresponding simulation value obtained by Boda *et al.*[35] Nevertheless, the present DFT results are still consistent with Ca^{2+} ion selectivity. The selectivity is due to the fact that a Ca^{2+} ion delivers twice the charge of a Na^+ ion while they occupy the same space and therefore it satisfies local charge neutrality more efficiently in the confined space of the filter. The present DFT results are in qualitative agreement with the simulation data in this case.

IV. CONCLUSIONS

The ion density distributions, separation factors, and exclusion coefficients of various electrolytes as well as mixed solution of MX_2-NX-H_2O inside a charged cylindrical nanopore have been investigated using a partially perturbative DFT. In the theory, the excess Helmholtz energy functional is constructed on the basis of the modified fundamental measure theory for the hard-core repulsion and a functional Taylor expansion of the charge contribution around the uniform reference fluid. The analytical expression of the direct correlation functions from the MSA is used as an input in the partially perturbative DFT. Large amounts of computer simulation data have been used to determine the range of validity of the partially perturbative DFT for these systems. The DFT results are compared with those from the PB equation and the comparisons suggest that the partially perturbative DFT be better than the classical PB equation under all conditions.

The PB equation predicts good ion density profiles and exclusion coefficients for the monovalent counterion systems at low bulk electrolyte concentration. This conclusion is the same as drawn from the electric double layers. The shortcomings of the PB equation are clearly seen in the predicted ion density profiles, separation factors, and exclusion coefficients for the multivalent counterion systems. The PB equation is qualitatively and quantitatively wrong in the prediction for multivalent counterion systems at high bulk electrolyte concentration and high surface charge density. The significant discrepancies between the PB equation and the simulations can be interpreted as a result of neglecting interionic and steric effects in the classical theory. This is confirmed by the predictions of the partially perturbative DFT, which includes the interionic correlations in a perturbative way.

The partially perturbative DFT proposed in this work accurately predicts the ion density distributions and separation factors of various electrolyte solutions inside the charged cylindrical nanopores. The exclusion coefficients from the present DFT are in good agreement with those from the GCMC simulations for the systems studied. The present DFT can be used to predict the selectivity of a calcium channel while the results are qualitatively right.

The physical model applied in this work is the restricted primitive model of electrolyte. It neglects the molecular nature of the solvent and the effect of the dielectric boundary. But the GCMC simulation of the solvent primitive model indicates that the addition of a neutral solvent yields more structural local concentration profiles of ions and has little influence on the volume-averaged quantities. Consequently, the thermodynamic results obtained from the primitive model are confident of practical applications. In addition, the partially perturbative DFT proposed in this work can be directly extended to the arbitrary mixed electrolyte solution inside a charged cylindrical nanopore using the direct correlation functions of the MSA for ions with different sizes and valences.

ACKNOWLEDGMENTS

We would like to make an acknowledgment to Yong-Jun Du for typing the manuscript. The authors greatly appreciate the financial supports of National Natural Science Foundation of China (Grant Nos. 20676065 and 20736003), Specialized Research Fund for the Doctoral Program of Higher Education (Grant No. 20070003099), and the Program for New Century Excellent Talents in University (NCET) of China.

APPENDIX: INTEGRATION OF SECOND DIRECT CORRELATION FUNCTION TERM

The integral of second direct correlation function term in Eq. (20) can be expressed as

$$
\begin{aligned}
I &= \int \Delta C_{ij}^{(2)el}(|\mathbf{r}'-\mathbf{r}|)\rho_j(\mathbf{r}')\theta(\sigma-|\mathbf{r}'-\mathbf{r}|)d\mathbf{r}' \\
&= \int -\frac{z_i z_j e^2\beta}{4\pi\varepsilon_0\varepsilon}\left[\frac{2B}{\sigma}-\left(\frac{B}{\sigma}\right)^2|\mathbf{r}'-\mathbf{r}|-\frac{1}{|\mathbf{r}'-\mathbf{r}|}\right] \\
&\quad \times\rho_j(\mathbf{r}')\theta(\sigma-|\mathbf{r}'-\mathbf{r}|)d\mathbf{r}' \\
&= -\frac{z_i z_j e^2\beta}{4\pi\varepsilon_0\varepsilon}\left[\frac{2B}{\sigma}I_1-\left(\frac{B}{\sigma}\right)^2 I_2-I_3\right], \qquad \text{(A1)}
\end{aligned}
$$

where

$$I_1 = 4\sigma^3 \int_0^{\pi} d\phi \int_0^{\pi/2} d\gamma \rho_j(r') \sin\gamma \cos^2\gamma, \quad \text{(A2)}$$

$$I_2 = \frac{\sigma}{2} I_1 + 2\sigma^4 \int_0^{\pi} d\phi \int_0^{\pi/2} d\gamma \rho_j(r') \sin^3\gamma \cos\gamma \ln(1+\cos\gamma), \quad \text{(A3)}$$

$$I_3 = 4\sigma^2 \int_0^{\pi} d\phi \int_0^{\pi/2} d\gamma \rho_j(r') \sin\gamma \cos\gamma \ln(1+\cos\gamma), \quad \text{(A4)}$$

with

$$r' = \sqrt{r^2 + (\sigma \sin\gamma)^2 - 2r\sigma \sin\gamma \cos\phi}. \quad \text{(A5)}$$

The integrals I_1, I_2, and I_3 can be integrated numerically using the Gauss method.

[1] D. Henderson, *Fundamentals of Inhomogeneous Fluids* (Marcel Dekker, New York, 1992).
[2] G. Jacazio, R. F. Probstein, A. A. Sonin, and D. Yung, J. Phys. Chem. **76**, 4015 (1972); S. Fu, Y.-X. Yu, and X.-L. Wang, Acta Chimi. Sin. **65**, 923 (2007).
[3] M. Higa, A. Kira, A. Tanioka, and K. Miyasaka, J. Chem. Soc., Faraday Trans. **89**, 3433 (1993).
[4] S. Mohanty and A. W. McCormick, Chem. Eng. J. **74**, 1 (1999).
[5] S. Heinemann, H. Terlau, W. Stuhmer, K. Imoto, and S. Numa, Nature (London) **356**, 441 (1992).
[6] B. Jamnik and V. Vlachy, J. Am. Chem. Soc. **115**, 660 (1993).
[7] B. Jamnik and V. Vlachy, J. Am. Chem. Soc. **117**, 8010 (1995).
[8] V. Vlachy, Langmuir **17**, 399 (2001).
[9] V. Vlachy and A. D. J. Haymet, J. Am. Chem. Soc. **111**, 477 (1989).
[10] D. Goulding, J.-P. Hansen, and S. Melchionna, Phys. Rev. Lett. **85**, 1132 (2000).
[11] D. Boda, D. Henderson, and D. D. Busath, J. Phys. Chem. B **105**, 11574 (2001).
[12] T. W. Allen, S. Kunyucak, and S. H. Chung, J. Chem. Phys. **111**, 7985 (1999); W. Y. Lo and K. Y. Chan, Mol. Phys. **86**, 745 (1995); S. T. Cui and H. D. Cochran, J. Chem. Phys. **117**, 5850 (2002); W. Im, S. Seefeld, and B. Roux, Biophys. J. **79**, 788 (2000).
[13] F. G. Donnan, Zeitschrift für Elektrochemie **17**, 572 (1911).
[14] K. A. Kraus, A. E. Marcinkowsky, J. S. Johnson, and A. J. Shor, Science **151**, 194 (1966).
[15] Y. Kobatake, J. Chem. Phys. **28**, 146 (1958); **28**, 442 (1958); F. A. Morrison, Jr., and J. F. Osterle, *ibid.* **43**, 2111 (1965).
[16] B. Hribar, V. Vlachy, L. B. Bhuiyan, and C. W. Outhwaite, J. Phys. Chem. B **104**, 11522 (2000).
[17] L. Yeomans, S. E. Feller, E. Sanchez, and M. Lozada-Cassou, J. Chem. Phys. **98**, 1436 (1993); G. E. Aguilar-Pineda, F. Jimenez-Angeles, J. Yu, and M. Lozada-Cassou, J. Phys. Chem. B **111**, 2033 (2007); P. Zaini, H. Modarress, and G. A. Mansoori, J. Chem. Phys. **104**, 3832 (1996).
[18] D. Busath, D. Henderson, and S. Sokolowski, J. Phys.: Condens. Matter **16**, S2193 (2004).
[19] J. Pinero, L. B. Bhuiyan, J. Rescic, and V. Vlachy, J. Chem. Phys. **127**, 104904 (2007).
[20] L. Blum and A. J. Torruella, J. Chem. Phys. **56**, 303 (1972).
[21] Y.-X. Yu, J. Z. Wu, and G.-H. Gao, Chin. J. Chem. Eng. **12**, 688 (2004); C. N. Patra and S. K. Ghosh, J. Chem. Phys. **117**, 8938 (2002).
[22] Y.-X. Yu, J. Wu, and G.-H. Gao, J. Chem. Phys. **120**, 7223 (2004).
[23] K. Wang, Y.-X. Yu, and G.-H. Gao, Phys. Rev. E **70**, 011912 (2004).
[24] K. Wang, Y.-X. Yu, and G.-H. Gao, J. Chem. Phys. **128**, 185101 (2008); C. N. Patra and A. Yethiraj, J. Phys. Chem. B **103**, 6080 (1999); T. Goel, C. N. Patra, S. K. Ghosh, and T. Mukherjee, J. Chem. Phys. **129**, 154906 (2008).
[25] Y.-X. Yu and J. Z. Wu, J. Chem. Phys. **117**, 10156 (2002).
[26] Y. Rosenfeld, J. Chem. Phys. **98**, 8126 (1993).
[27] K. Wang, Y.-X. Yu, G.-H. Gao, and G.-S. Luo, J. Chem. Phys. **123**, 234904 (2005).
[28] T. Boublik, J. Chem. Phys. **53**, 471 (1970); N. F. Carnahan and K. E. Starling, *ibid.* **51**, 635 (1969).
[29] Y. Rosenfeld, Phys. Rev. Lett. **63**, 980 (1989).
[30] E. Waisman and J. L. Lebowitz, J. Chem. Phys. **56**, 3086 (1972); **56**, 3093 (1972).
[31] L. Blum, J. Stat. Phys. **22**, 661 (1980).
[32] P. Barak, J. Colloid Interface Sci. **133**, 479 (1989).
[33] A. Lehmani, O. Bernard, and P. Turq, J. Stat. Phys. **89**, 379 (1997).
[34] K. Hiroike, Mol. Phys. **33**, 1195 (1977).
[35] D. Boda, D. D. Busath, D. Henderson, and S. Sokolowski, J. Phys. Chem. B **104**, 8903 (2000).